Available online at www.sciencedirect.com
ScienceDirect
Journal of Computational Physics 218 (2006) 275–294
JOURNAL OF COMPUTATIONAL PHYSICS
www.elsevier.com/locate/jcp

The dominant wave-capturing flux: A finite-volume scheme without decomposition for systems of hyperbolic conservation laws

Michael G. Edwards *

Civil and Computational Engineering Centre, School of Engineering, University of Wales Swansea, Singleton Park, Swansea, Wales SA2 8PP, United Kingdom

Received 25 August 2004; received in revised form 7 February 2006; accepted 8 February 2006
Available online 29 March 2006

Abstract

More robust developments of schemes for hyperbolic systems, that avoid dependence upon a characteristic decomposition have been achieved by employing schemes that are based on a Rusanov flux. Such schemes permit the construction of higher order approximations without recourse to characteristic decomposition. This is achieved by using the maximum eigenvalue of the hyperbolic system within the definition of the numerical flux. In recent literature the Rusanov flux has been embedded in a local Lax–Friedrichs flux. The current literature on these schemes only appears to indicate success in this regard, with no investigation of the effect of the additional numerical diffusion that is inherent in such formulations.

In this paper the foundation for a new scheme is proposed which relies on the detection of the dominant wave in the system. This scheme is designed to permit the construction of lower and higher order approximations without recourse to characteristic decomposition while avoiding the excessive numerical diffusion that is inherent in the Rusanov and local Lax–Friedrichs fluxes.

MSC: 65M06; 65M50

Keywords: Finite-volume; Higher order; Dominant wave; Rusanov; Lax–Friedrichs

1. Introduction

Many locally conservative schemes have been developed for systems of hyperbolic conservation laws [1]. The most successful high resolution schemes, in terms of actual front resolution, depend upon a characteristic decomposition of the system. The decomposition leads to optimal upwind schemes where upwind directions can be resolved according to the characteristic wave components and upwind approximations applied with minimum dissipation. Roe's approximate Riemann solver [2] is one of the most popular schemes of this type.

* Tel.: +44 1792 513175.
E-mail address: m.g.edwards@swansea.ac.uk.

0021-9991/$ - see front matter
doi:10.1016/j.jcp.2006.02.005

The method has excellent shock capturing capabilities, while the method requires an entropy fix to disperse expansion shocks, it remains one of the most efficient decomposition schemes when compared to rival formulations.

However, the discovery of a scheme that can provide front resolution that is comparable with that of the best upwind schemes, while avoiding the need for characteristic decomposition continues to present a major challenge in this area, e.g. [3].

The standard approach to this problem, particularly for steady-state problems, involves employing schemes that are essentially "central difference" in character, e.g. [5], together with some form of artificial dissipation, e.g. [4,6–8]. Earlier finite element schemes were also developed along these lines, e.g. [9].

More robust developments of schemes for systems, that avoid dependence upon a characteristic decomposition have been achieved by employing some form of a Lax–Friedrichs flux [12] or Rusanov [18] based flux, e.g. [10,11,3] and more recently [13–15]. In these schemes, the dependency upon the characteristic components is removed by using the modulus of maximum eigenvalue of the hyperbolic system within the definition of the numerical flux. Such schemes then permit the construction of higher order approximations without recourse to characteristic decomposition. The more recent schemes [13–15] employ a modified form of Rusanov flux that depends on the maximum eigenvalue of the hyperbolic system within a local (or global) Lax–Friedrichs flux (LLF). The recent literature on these schemes only appears to indicate success in this regard, with little apparent investigation of the effect of the additional numerical diffusion that is inherent in such formulations.

In this paper the foundation for a new scheme is proposed which relies on the detection of the dominant wave in the system [16,17]. This scheme is designed to permit the construction of lower and higher order approximations without recourse to characteristic decomposition while avoiding the excessive numerical diffusion that is inherent within the Rusanov and local Lax–Friedrichs based flux approximations.

This paper describes the motivation and derivation of the dominant wave capturing technique. The formulation ensures that local conservation is maintained and is developed within a general finite volume framework where a comparison with Rusanov and the Lax–Friedrichs flux is also presented. Low order and higher order versions of the method are presented on structured and unstructured grids.

The application includes the Euler equations of compressible flow. Comparisons between the new method and the Rusanov and LLF schemes reveal clear weaknesses of the Rusanov and LLF based formulations. Some classical flow problems are presented where the Rusanov and LLF schemes fail to detect discontinuities that are known to be present in the physical solution. In contrast, the new dominant wave scheme is able to capture the discontinuities while using exactly the same grids and equivalent levels of accuracy in terms of polynomial approximation. The results presented demonstrate the benefits of the dominant wave formulation, for both low order and higher order approximations on structured and unstructured grids.

Finally, it is noted that the dominant wave formulation offers the benefits of being directly applicable to other systems of hyperbolic conservation laws without requiring a characteristic decomposition.

2. Flow equations

The schemes presented here are applicable to hyperbolic systems of the form

$$\int_{\Omega} \frac{\partial \mathbf{u}}{\partial t}\,\mathrm{d}V + \int_{\Omega} \frac{\partial \mathbf{F}(\mathbf{u})}{\partial x} + \frac{\partial \mathbf{G}(\mathbf{u})}{\partial y}\,\mathrm{d}V = 0 \tag{1}$$

where the integral is over volume Ω. The Euler equations of compressible flow are considered in this paper with:

$$\begin{aligned} \mathbf{u} &= (\rho, \rho u, \rho v, E)^{\mathrm{T}} \\ \mathbf{F}(\mathbf{u}) &= (\rho u, \rho u^2 + p, \rho uv, u(E+p))^{\mathrm{T}} \\ \mathbf{G}(\mathbf{u}) &= (\rho v, \rho uv, \rho v^2 + p, v(E+p))^{\mathrm{T}} \end{aligned} \tag{2}$$

Here ρ, p and E are the density, pressure and energy per unit volume of an ideal gas $\mathbf{q} = (u,v)$ the Cartesian components of velocity and

$$E = \rho\left[\frac{1}{2}q^2 + p/\rho(\gamma - 1)\right] \tag{3}$$

γ being the ratio of specific heat capacities, $q^2 = u^2 + v^2$ and sound speed $a = \sqrt{\gamma p/\rho}$.

2.1. Boundary conditions

For the initial value problem (IVP) field data is prescribed. For initial boundary value problems (IBVP), considered here in two-dimensions, an initial flow field is prescribed together with boundary values which are assigned according to the number of inward pointing characteristics, e.g. [1] for further discussion. Zero normal flow is imposed on solid walls. For the Euler equations, on a solid wall the Euler flux reduces to being a function of pressure.

3. Approximate Riemann solvers with upwinding

3.1. Scalar equation

First we consider the one-dimensional scalar equation

$$\frac{\partial u}{\partial t} + \frac{\partial F(u)}{\partial x} = 0 \tag{4}$$

which is to be solved over the domain $[a, b]$ with initial data $u(x,0) = u_0(x)$. We define the numerical schemes for integrating Eq. (4) on a computational grid in one spatial dimension with discrete nodes $x_i = i\Delta x$ and time at level n where $t^n = n\Delta t$. The standard first order explicit upwind scheme can be written as

$$u_i^{n+1} = u_i^n - \frac{\Delta t}{\Delta x}\left(f^n_{i+\frac{1}{2}} - f^n_{i-\frac{1}{2}}\right) \tag{5}$$

where forward Euler time integration is used and the approximate numerical flux is defined by

$$f^n_{i+\frac{1}{2}} = \frac{1}{2}\left(F(u^n_{i+1}) + F(u^n_i) - \left|\lambda_{i+\frac{1}{2}}\right|(u^n_{i+1} - u^n_i)\right) \tag{6}$$

and

$$\lambda_{i+\frac{1}{2}} = \begin{cases} (F(u^n_{i+1}) - F(u^n_i))/(u^n_{i+1} - u^n_i) & |(u^n_{i+1} - u^n_i)| > \epsilon \\ \partial F(u)/\partial u & |(u^n_{i+1} - u^n_i)| \leqslant \epsilon \end{cases} \tag{7}$$

where ϵ is an appropriate tolerance to prevent a zero divide. This definition of wave speed ensures that shocks are captured with precision for any finite jump in u, with $\lambda_{i+\frac{1}{2}}$ assuming the Rankine–Hugoniot shock speed across a mesh interval. In this form the first order spatial scheme appears as a central scheme comprised of a central difference in flux together with a central difference of a diffusion term. The scheme can be seen in its original upwind form by noting that for a positive wave speed the flux uses data to the left and reduces to $f_{i+\frac{1}{2}} = F(u^n_i)$, otherwise $f_{i+\frac{1}{2}} = F(u^n_{i+1})$ and the flux uses data to the right. While the definition of Eqs. (5)–(7) does not require any explicit sign dependence in the scheme, the upwind directions are clearly detected. This explicit scheme is the most fundamental scheme for scalar conservation laws in one dimension and is stable and monotonicity preserving subject to a maximum CFL condition of unity. This scheme also requires an entropy fix to disperse expansion shocks [19].

3.2. Systems

We now turn to systems of hyperbolic conservation laws of the form

$$\frac{\partial \mathbf{u}}{\partial t} + \frac{\partial \mathbf{F}(\mathbf{u})}{\partial x} = 0 \tag{8}$$

defined over the domain interval $[a,b]$ subject to initial data $\mathbf{u}(x,0) = \mathbf{u}_0(x)$. The vector $\mathbf{u}$ has N components and the system Jacobian matrix $A = \partial\mathbf{F}/\partial\mathbf{u}$ has N real eigenvalues. In order to apply upwind schemes of the type described above to a system of the form given in Eq. (1) the system is first decomposed into characteristic form via the transformation

$$\Delta\mathbf{u} = R\Delta\mathbf{v} \tag{9}$$

where R is the matrix of right eigenvectors of the system Jacobian matrix A, the matrix of eigenvalues Λ is defined via

$$AR = R\Lambda \tag{10}$$

and $\Delta\mathbf{u}$, $\Delta\mathbf{v}$ represent the respective conservative and characteristic variable increments. The upwind scheme is in effect applied to each characteristic wave component and the discrete system is recomposed into conservation form. The first order scheme for a system is written as

$$\mathbf{u}_i^{n+1} = \mathbf{u}_i^n - \frac{\Delta t}{\Delta x}\left(\mathbf{f}_{i+\frac{1}{2}}^n - \mathbf{f}_{i-\frac{1}{2}}^n\right) \tag{11}$$

where the approximate flux is defined by

$$\mathbf{f}_{i+\frac{1}{2}}^n = \frac{1}{2}\left(\mathbf{F}\left(\mathbf{u}_{i+1}^n\right) + \mathbf{F}\left(\mathbf{u}_i^n\right) - R\left|\Lambda_{i+\frac{1}{2}}\right|R^{-1}\left(\mathbf{u}_{i+1}^n - \mathbf{u}_i^n\right)\right) \tag{12}$$

and the definition of the discrete eigenvalues $\lambda_{i+\frac{1}{2}}$ now require an appropriate generalization of Eq. (7) such that conservation together with the exact shock speed are maintained. This is the basis of the Roe scheme [2], however, as in the scalar case a (non-linear) componentwise entropy fix is required to disperse expansion shocks [19]. The CFL condition now applies with respect to the maximum eigenvalue of the system.

4. Approximate Riemann solvers without upwinding in one dimension

The appearance of the matrix of eigenvectors R in the system flux approximation of Eqs. (11) and (12) is a consequence of upwinding on each characteristic component. This scheme has an optimal diffusive operator in terms of numerical diffusion (though relatively complicated by the entropy fix) provided the shock jump criteria can be satisfied for the system in hand. If the matrix of eigenvalues is proportional to the unit matrix (equal eigenvalues) then the dependency of the discrete flux on the matrix of eigenvectors is removed leaving a much simpler diffusion coefficient which is independent of characteristic decomposition.

The upwind scheme can be simplified in this way without appearing to violate the crucial monotonicity preserving property of the scheme, subject to the CFL condition, by replacing the diagonal matrix of absolute eigenvalues $|\Lambda|$ evaluated at $i+\frac{1}{2}$ with the matrix $|\Lambda_{\mathrm{RUS}}| = \left|\lambda_{\mathrm{RUS}\,i+\frac{1}{2}}\right| I$ where

$$\left|\lambda_{\mathrm{RUS}\,i+\frac{1}{2}}\right| = \left(\max_j \left|\lambda_{i+\frac{1}{2}}^j\right|\right) \tag{13}$$

which depends on the maximum eigenvalue of the system and leads to the Rusanov flux [18]

$$\mathbf{f}_{i+\frac{1}{2}}^n = \frac{1}{2}\left(\mathbf{F}\left(\mathbf{u}_{i+1}^n\right) + \mathbf{F}\left(\mathbf{u}_i^n\right) - |\Lambda_{\mathrm{RUS}}|\left(\mathbf{u}_{i+1}^n - \mathbf{u}_i^n\right)\right) \tag{14}$$

where it is understood that $|\Lambda_{\mathrm{RUS}}|$ is defined at the interface $i+\frac{1}{2}$, here the Roe average is used. The scheme proposed in [13] embeds the Rusanov flux within the LLF flux yielding an LLF flux for systems defined by:

$$\begin{aligned}
&\mathbf{f}_{i+\frac{1}{2}}^n = \frac{1}{2}\left(\mathbf{F}(\mathbf{u}_{i+1}^n) + \mathbf{F}(\mathbf{u}_i^n) - |\Lambda_{\mathrm{LLF}}|(\mathbf{u}_{i+1}^n - \mathbf{u}_i^n)\right)\\
&\left|\lambda_{\mathrm{LLF}i+\frac{1}{2}}\right| = \max_{x_{\mathrm{L}},x_{\mathrm{R}}}\left(\max_j \left|\lambda_{i+\frac{1}{2}}^j\right|\right)
\end{aligned} \tag{15}$$

where $|\Lambda_{\mathrm{LLF}}| = \left|\lambda_{\mathrm{LLF}i+\frac{1}{2}}\right| I$. The system LLF flux therefore depends on the maximum eigenvalue of the system over the local interval $[x_i,x_{i+1}]$. A global version of the latter scheme for systems can be defined with flux:

$$\begin{aligned}\mathbf{f}^n_{i+\frac{1}{2}} &= \frac{1}{2}\left(\mathbf{F}\left(\mathbf{u}^n_{i+1}\right) + \mathbf{F}\left(\mathbf{u}^n_i\right) - |\Lambda_{\mathrm{GLF}}|\left(\mathbf{u}^n_{i+1} - \mathbf{u}^n_i\right)\right)\\ \left|\lambda_{\mathrm{GLF}i+\frac{1}{2}}\right| &= \max_{x_a,x_b}\left(\max_j\left|\lambda^j_{i+\frac{1}{2}}\right|\right)\end{aligned} \tag{16}$$

where $|\Lambda_{\mathrm{GLF}}| = \left|\lambda_{\mathrm{GLF}i+\frac{1}{2}}\right| I$ and the system GLF flux depends on the maximum eigenvalue of the system over the domain $[x_a,x_b]$, e.g. [15,14].

Note that the schemes are locally conservative. Extension to higher order accuracy is discussed in Section 7. Since all eigenvalues in the diffusion component of upwind flux are replaced by their maximum modulus to obtain the Rusanov flux, it follows that the price to be paid for this simplification is extra numerical diffusion. Since the LLF flux uses a further maximum over the interval (compared to Rusanov), it follows that the entropy satisfying LLF scheme will have diffusion greater than or equal to that of the Rusanov scheme. Moreover the GLF scheme's dependence on the maximum over the domain will yield diffusion greater than or equal to that of LLF. There is little discussion in the literature on the effect of the additional diffusion on the (low or higher order) results in terms of dissipation. There is a report that this scheme can be accompanied by further oscillations unless the global maximum eigenvalue over the domain is employed [15]. The following section presents an alternative non-upwind scheme which is quite different to the above three schemes, and relies on detecting the dominant wave of the system.

5. Dominant wave of a system of hyperbolic conservation laws

The notion of a dominant wave arises when attempting to describe a system of hyperbolic conservation laws with just a single *best* characteristic [16]. In order to illustrate the construction, it is necessary to introduce the mobile operator that measures total rate of change in time along the characteristic as

$$\frac{\mathrm{D}\mathbf{u}}{\mathrm{D}t} = \frac{\partial \mathbf{u}}{\partial t} + \frac{\mathrm{D}x}{\mathrm{D}t}\frac{\partial \mathbf{u}}{\partial x} \tag{17}$$

The system

$$\frac{\partial \mathbf{u}}{\partial t} + \frac{\partial \mathbf{F}(\mathbf{u})}{\partial x} = 0 \tag{18}$$

can then be expressed in terms of the mobile operator as

$$\frac{\mathrm{D}\mathbf{u}}{\mathrm{D}t} = \frac{\mathrm{D}x}{\mathrm{D}t}\frac{\partial \mathbf{u}}{\partial x} - \frac{\partial \mathbf{F}(\mathbf{u})}{\partial x} \tag{19}$$

For a scalar equation the characteristic is defined by equating the right hand side of Eq. (19) to zero. In order to define the best single characteristic of a system, the L_2 norm

$$\left\|\frac{\mathrm{D}\mathbf{u}}{\mathrm{D}t}\right\|_2 = \left\|\frac{\mathrm{D}x}{\mathrm{D}t}\frac{\partial \mathbf{u}}{\partial x} - \frac{\partial \mathbf{F}(\mathbf{u})}{\partial x}\right\|_2 \tag{20}$$

of the total rate of change is instead minimized over $\mathrm{D}x/\mathrm{D}t$. This leads to the generalized wave velocity

$$\frac{\mathrm{D}x}{\mathrm{D}t} = \frac{\partial \mathbf{u}}{\partial x}\cdot\frac{\partial \mathbf{F}(\mathbf{u})}{\partial x}\Big/\frac{\partial \mathbf{u}}{\partial x}\cdot\frac{\partial \mathbf{u}}{\partial x} \tag{21}$$

with orthogonality such that

$$\frac{\mathrm{D}\mathbf{u}}{\mathrm{D}t}\cdot\frac{\partial \mathbf{u}}{\partial x} = 0 \tag{22}$$

The generalized wave reduces to the *exact* characteristic for a scalar wave equation. The wave speed of Eq. (21) has been shown to be approximately proportional to the dominant wave eigenvalue of the system [16]. This can be seen by invoking Eqs. (9) and (10) in (21) to yield

$$\frac{\mathrm{D}x}{\mathrm{D}t} = \left(\frac{\partial \mathbf{v}^{\mathrm{T}}}{\partial x}R^{\mathrm{T}}R\Lambda\frac{\partial \mathbf{v}}{\partial x}\right)\Big/\left(\frac{\partial \mathbf{v}^{\mathrm{T}}}{\partial x}R^{\mathrm{T}}R\frac{\partial \mathbf{v}}{\partial x}\right) \tag{23}$$

which is therefore approximately proportional to the eigenvalue corresponding to the strongest wave strength in characteristic gradient, and proves to be an optimal choice for a system when selecting a single wave speed.

6. Dominant wave scheme

The discrete dominant wave speed denoted here by λ_{DW} is naturally defined by

$$\lambda_{\mathrm{DW}} = ((\mathbf{u}_{\mathrm{R}} - \mathbf{u}_{\mathrm{L}}) \cdot (\mathbf{F}_{\mathrm{R}} - \mathbf{F}_{\mathrm{L}}))/((\mathbf{u}_{\mathrm{R}} - \mathbf{u}_{\mathrm{L}}) \cdot (\mathbf{u}_{\mathrm{R}} - \mathbf{u}_{\mathrm{L}})) \tag{24}$$

which is a function of differences between left and right states L and R, respectively. This definition is consistent with Eq. (7), for a scalar equation this definition reduces to the discrete wave speed of Eq. (7) for any finite jump in u. An immediate advantage of this definition of wave speed is the independence from a characteristic decomposition. In addition to detecting the system dominant wave, in the limit this definition equates to the exact shock speed for any wave type. This can be seen by employing the Rankine–Hugoniot shock jump relationship [27]

$$(\mathbf{F}_{\mathrm{R}} - \mathbf{F}_{\mathrm{L}}) = \sigma(\mathbf{u}_{\mathrm{R}} - \mathbf{u}_{\mathrm{L}}) \tag{25}$$

where σ is the shock speed, substituting for the flux jump defined by Eq. (25) into Eq. (24) yields

$$\lambda_{\mathrm{DW}} = \sigma \tag{26}$$

This is a further property that is not possessed by other definitions of artificial viscosity coefficients (other than the Roe scheme), including the above Rusanov based schemes unless the Roe definition of eigenvalue is employed and the shock corresponds with the maximum eigenvalue. The discrete dominant wave flux is now defined by

$$\mathbf{f}^n_{i+\frac{1}{2}} = \frac{1}{2}\left(\mathbf{F}\left(\mathbf{u}^n_{i+1}\right) + \mathbf{F}\left(\mathbf{u}^n_i\right) - |\Lambda_{\mathrm{DW}}|\left(\mathbf{u}^n_{i+1} - \mathbf{u}^n_i\right)\right) \tag{27}$$

where

$$|\Lambda_{\mathrm{DW}}| = |\lambda_{\mathrm{DW}}| I \tag{28}$$

and $|\lambda_{\mathrm{DW}}|$ is defined by Eq. (24). The dominant wave scheme is then defined be Eqs. (24), (27) and (11) and the scheme is locally conservative by construction.

6.1. Stability and dominant wave bounds

Although formal stability of the dominant wave scheme cannot be proven the scheme may retain stability whenever a particular wave dominates the system, due to the above observation that the dominant wave speed is then approximately proportional to the corresponding dominant wave eigenvalue. In addition the wave speed will adapt approximately to the local dominant wave of the flow in different regions of the flow field as the solution evolves in time.

In cases where there is no dominant wave the scheme may require modification in the form of additional viscosity. One option is to choose a convex average of the absolute dominant wave speed and absolute maximum eigenvalue. In this section we consider how to modify the scheme such that consistency with the formulation is maintained and avoid additional arbitrary artificial viscosity.

First we note that for a symmetric system Jacobian matrix, Eq. (24) reduces to

$$\frac{\mathrm{D}x}{\mathrm{D}t} = \left(\frac{\partial \mathbf{v}^{\mathrm{T}}}{\partial x} \Lambda \frac{\partial \mathbf{v}}{\partial x}\right) \Big/ \left(\frac{\partial \mathbf{v}^{\mathrm{T}}}{\partial x} \frac{\partial \mathbf{v}}{\partial x}\right) \tag{29}$$

and in this case the dominant wave satisfies the inequalities

$$\min_j \lambda^j \leqslant \lambda_{\mathrm{DW}} \leqslant \max_j \lambda^j \tag{30}$$

We note that if entropy variables are used Eq. (30) holds immediately. In this work our focus is on a conservative variable formulation. Since we are interested in the modulus of wave speed when formulating the

scheme (Eq. (27)), we use Eq. (30) to motivate the imposition of bounds on the discrete dominant wave speed such that

$$\min_j |\lambda^j| \leqslant |\lambda_{\mathrm{DW}}| \leqslant \max_j |\lambda^j| \tag{31}$$

The bounds of Eq. (31) ensure that the discrete dominant wave speed remains within the physical eigenvalue limits. Indeed for the Euler equations the bounds applied here are

$$|u - a| \leqslant |\lambda_{\mathrm{DW}}| \leqslant |u + a| \tag{32}$$

and are achieved by defining the bounded dominant wave speed $|\lambda_{\mathrm{DWB}}|$ via

$$|\lambda_{\mathrm{DWB}}| = \min(\max(|u - a|, |\lambda_{\mathrm{DW}}|), |u + a|) \tag{33}$$

The practical effects of the bounds are discussed in Section 10, but some comments are appropriate here. An important point is that the dominant wave scheme together with the bounds Eq. (32) in 1-D, (the 2-D form is presented later in the paper) is found to perform successfully for all test cases presented. However, it is also found that the bounds are not necessary for all test cases and when they are necessary it is observed that the lower bound enhances stability, which is consistent with an increase in local viscosity compared to the dominant wave. Therefore, the bounded dominant wave speed $|\lambda_{\mathrm{DWB}}|$ is defined by

$$|\lambda_{\mathrm{DWB}}| = \max(|u - a|, |\lambda_{\mathrm{DW}}|) \tag{34}$$

Further discussion is given in Section 10.

Finally we note that the definition of wave speed in Eq. (24) is singular unless there exists a non-zero finite jump or difference between left and right states. Currently, in this event the maximum eigenvalue is used. Numerical differentiation is a further possibility in such cases where Eq. (24) is singular and would retain complete independence from a characteristic decomposition although this has not been used to date.

7. Higher order schemes without upwinding in one dimension

In the scalar case a higher order approximation is applied to the conservation variable. When an upwind scheme is applied to a system the higher order approximation is typically introduced wave by wave and applied to the characteristic variables, followed by recomposition to the conservative variables. In contrast, when using any of the discrete Rusanov based fluxes of Eqs. (14)–(16), respectively, or the dominant wave flux defined by Eq. (27), the extension to higher order accuracy is simpler to achieve with the non-upwind formulations when applied to systems, since there is no dependency upon characteristic variables in these definitions of flux. Consequently, a higher order approximation can be introduced for the left and right states, respectively, and be expressed directly in terms of the conservative variables. Alternatively the higher order expansions can also be applied to other sets of variables such as primitive or characteristic variables. In this work the conservative variables are used directly.

In one dimension the scheme is expressed as a two-step process. First the higher order states are defined using a MUSCL formalism [20]. Higher order left and right hand side states are obtained by expansions about the states L and R, viz:

$$\begin{aligned} \mathbf{u}_{\mathrm{L}i+\frac{1}{2}} &= \mathbf{u}_i + \frac{1}{2}\Phi(\mathbf{r}^+_{i+1/2})(\mathbf{u}_{i+1} - \mathbf{u}_i) \\ \mathbf{u}_{\mathrm{R}i+\frac{1}{2}} &= \mathbf{u}_{i+1} - \frac{1}{2}\Phi(\mathbf{r}^-_{i+1/2})(\mathbf{u}_{i+1} - \mathbf{u}_i) \end{aligned} \tag{35}$$

where $\Phi\left(\mathbf{r}^+_{i+1/2}\right)$ and $\Phi\left(\mathbf{r}^-_{i+1/2}\right)$ are flux limiters, or in this case slope limiters [20]. The slope limiters are functions of adjacent discrete gradients where $\mathbf{r}^+_{i+1/2} = (\Delta\mathbf{u}_{i-1/2}/\Delta\mathbf{u}_{i+1/2})$ and $\mathbf{r}^-_{i+1/2} = (\Delta\mathbf{u}_{i+3/2}/\Delta\mathbf{u}_{i+1/2})$ and $\Delta\mathbf{u}_{i+1/2} = \mathbf{u}_{i+1} - \mathbf{u}_i$. The slope limiters constrain the expansions to ensure that the higher order data remains monotonic in the scalar case. Details can be found in [20,21]. The above fluxes of Eqs. (14)–(16) and (27) can now be applied to the higher order data so that a local generalized Riemann problem is resolved (approximately) with a higher order flux of the form

$$\mathbf{f}_{i+\frac{1}{2}} = \frac{1}{2}\left(\left(\mathbf{F}\left(\mathbf{u}^n_{\mathrm{R}_{i+\frac{1}{2}}}\right) + \mathbf{F}\left(\mathbf{u}^n_{\mathrm{L}_{i+\frac{1}{2}}}\right)\right) - |\Lambda_{\mathrm{d}}|\left(\mathbf{u}^n_{\mathrm{R}_{i+\frac{1}{2}}} - \mathbf{u}^n_{\mathrm{L}_{i+\frac{1}{2}}}\right)\right) \tag{36}$$

where $\Lambda_{\mathrm{d}} = \Lambda_{\mathrm{RUS}}$, $\Lambda_{\mathrm{d}} = \Lambda_{\mathrm{LLF}}$ and $\Lambda_{\mathrm{d}} = \Lambda_{\mathrm{GLF}}$ correspond to the respective Rusanov based schemes of Eqs. (14)–(16), respectively, and $\Lambda_{\mathrm{d}} = \Lambda_{\mathrm{DW}}$ corresponds to dominant wave scheme. Any of the fluxes can now be used to integrate the system via Eq. (11). The higher order spatial scheme as defined by Eqs. (35), (36) and (11), uses first order forward-Euler time stepping. The CFL condition of the scheme is dependent on the choice of limiter, typically an upper limit of 1/2 is selected. Extension to higher order time accuracy can be achieved with the second or third order Runge–Kutta schemes of [25] which preserve the spatial operator properties. The CFL limit reduces further in higher dimensions. Note that the first order flux is recovered if the limiters are set to zero.

8. Approximate Riemann solvers without upwinding in two dimensions

In this section we describe the basic first order scheme. The higher dimensional extension of the above scheme is based on a direct generalization of the one-dimensional discrete flux and described in Section 9. The flow equations of Section 2 are integrated in space and time over a discrete control-volume Ω with surface $\delta\Omega$ by direct use of the Gauss divergence theorem applied to yield a surface integral of divergence

$$\int_{\Omega} (\mathbf{u}(t+\Delta t) - \mathbf{u}(t))\,\mathrm{d}V = -\int_{\Delta t}\int_{\delta\Omega} (\mathbf{F}\,\mathrm{d}y - \mathbf{G}\,\mathrm{d}x)\,\mathrm{d}t \tag{37}$$

Discrete cell vertex approximations are developed for general unstructured grids comprised of quadrilateral and-or triangular cells. A control-volume is constructed around each grid vertex, by joining centres of cell edges that connect to a given vertex, to centres of the cells that share the common vertex. This gives rise to a polygonal control-volume surrounding each grid vertex, where each cell attached to the central vertex contributes two sub-cell faces to the control-volume. We shall denote the ith vertex control-volume by Ω_i and surface $\delta\Omega_i$. Referring to the typical control-volume shown in Fig. 1, two adjacent sub-cell faces (labelled 1 and 2) are attached to each interior edge that connects to the central vertex i, while only one sub-cell face is attached to a boundary edge. In this formulation the control-volume surface is defined with respect to cell edges. The pth edge has one if a boundary, or two if interior, sub-cell faces with respect to which the surface outward normal increments are defined. Consequently, control-volume surface increments have double indices $\Delta\mathbf{n}_{p,j} = (\Delta y_{p,j}, -\Delta x_{p,j})$ where p and j ($1 \leqslant j \leqslant 2$) are the respective edge and sub-cell face numbers.

Thus approximation of the surface integral of a flux function $(\mathbf{F}(\mathbf{u}), \mathbf{G}(\mathbf{u}))$ over the control-volume is defined by

$$\sum_{p=1}^{N_{\mathrm{E}}}\sum_{j=1}^{N_{\mathrm{S}}} \mathscr{F}_{p,j}(\mathbf{u})|\Delta\mathbf{n}_{p,j}| = \sum_{p}^{N_{\mathrm{E}}}\sum_{j=1}^{N_{\mathrm{S}}} (\mathbf{F}(\mathbf{u})\Delta y_{p,j} - \mathbf{G}(\mathbf{u})\Delta x_{p,j}) \tag{38}$$

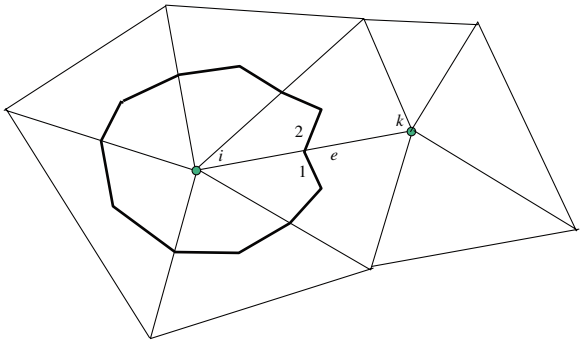

Fig. 1. Control-volume.

where the inner summation is over sub-cell faces j associated with edge p and $N_S = 2$ in the field and unity at a boundary. The outer summation is over the N_E control-volume edges connected to the central vertex i. The normal jth sub-cell face flux of edge p is defined by

$$\mathscr{F}_{p,j}(\mathbf{u}) = \frac{\mathbf{F}(\mathbf{u})\Delta y_{p,j} - \mathbf{G}(\mathbf{u})\Delta x_{p,j}}{|\Delta \mathbf{n}_{p,j}|} \tag{39}$$

As in one dimension the scheme is expressed as a two-step process: First discrete fluxes are defined on the control-volume faces, which are assembled in an edge-wise fashion. In the case of the first order scheme the first step simply involves selecting the left and right hand side states, which correspond to the left and right hand side edge vertex values of the conservation variables. An appropriate numerical flux must now be constructed.

8.1. Normally resolved Rusanov, LLF and GLF fluxes

In the case of the fluxes of Eqs. (13)–(16) their respective generalizations employ the directionally resolved outward normal flux of Eq. (39) which replaces the one-dimensional flux evaluated at the respective left and right hand states, so that edge based Riemann problems are resolved with the discrete generalized flux of the form

$$f_{p,j}(\mathbf{u}_R, \mathbf{u}_L) = \frac{1}{2}(\mathscr{F}_{p,j}(\mathbf{u}_R) + \mathscr{F}_{p,j}(\mathbf{u}_L) - |\Lambda_{d\,p,j}|(\mathbf{u}_R - \mathbf{u}_L)) \tag{40}$$

Now it will be understood that f, $\mathscr{F}$, Λ_d, $\hat{\mathbf{n}}$ each have the suffices p,j and they are omitted from the text. For the Euler equations the Rusanov flux is now defined by Eq. (40) with

$$|\Lambda_d| = \lambda_{RUS} = (|\mathbf{q}\cdot\hat{\mathbf{n}}| + a) \tag{41}$$

evaluated at the interval mid-point. The LLF flux is defined by Eq. (40) with

$$|\Lambda_d| = \lambda_{LLF} = \max_{L,R}(|\mathbf{q}\cdot\hat{\mathbf{n}}| + a) \tag{42}$$

where the maximum eigenvalue is taken over the local grid interval. The GLF flux is defined by Eq. (40) with

$$|\Lambda_d| = \lambda_{GLF} = \max_{\text{Domain}}(|\mathbf{q}\cdot\hat{\mathbf{n}}| + a) \tag{43}$$

where the maximum is taken over all grid intervals of the domain.

8.2. Normally resolved dominant wave flux

For the dominant wave scheme, the generalization of Eq. (27) is employed, again the directionally resolved outward normal flux of Eq. (39) replaces the one-dimensional flux evaluated at the respective left and right hand states. The dominant wave flux is defined by

$$f_{p,j}(\mathbf{u}_R, \mathbf{u}_L) = \frac{1}{2}(\mathscr{F}_{p,j}(\mathbf{u}_R) + \mathscr{F}_{p,j}(\mathbf{u}_L) - |\Lambda_{DW\,p,j}|(\mathbf{u}_R - \mathbf{u}_L)) \tag{44}$$

Again it is understood that f, $\mathscr{F}$, Λ_{DW}, $\hat{\mathbf{n}}$ bare the suffices p,j and they are omitted. The dominant wave speed is defined by a generalized form of Eq. (24), obtained by using the normally resolved flux of Eq. (39) in (24) and the speed is a function of left and right edge-vertex states with,

$$\lambda_{DW} = ((\mathbf{u}_R - \mathbf{u}_L)\cdot(\mathscr{F}(\mathbf{u}_R) - \mathscr{F}(\mathbf{u}_L)))/((\mathbf{u}_R - \mathbf{u}_L)\cdot(\mathbf{u}_R - \mathbf{u}_L)) \tag{45}$$

as before $\Lambda_{DW} = \lambda_{DW} I$. Note that this definition applies to *any* hyperbolic system. In two dimensions a bounding procedure analogous to Eqs. (31) and (32) can be imposed. In particular for the Euler equations, the bounds are defined such that

$$\|\mathbf{q}\cdot\hat{\mathbf{n}}| - a| \leqslant |\lambda_{DW}| \leqslant \|\mathbf{q}\cdot\hat{\mathbf{n}}| + a| \tag{46}$$

As stated above current tests show that the lower bound is sufficient in all cases and is imposed such that

$$|\lambda_{\mathrm{DWB}}| = \max(|\|\mathbf{q}\cdot\hat{\mathbf{n}}| - a|, |\lambda_{\mathrm{DW}}|) \tag{47}$$

where now $\Lambda_{\mathrm{DW}} = \lambda_{\mathrm{DWB}} I$ in Eq. (44). Further details are given in Section 10.

8.3. Explicit first order scheme

The second step of the non-upwind scheme formulation involves formal time integration of the fully discrete divergence of flux for each component of the system, which is shown below with forward-Euler time integration. The discrete scheme for vertex i (control-volume area ΔA_i) can then be written as

$$\mathbf{u}_i^{n+1} = \mathbf{u}_i^n - \frac{\Delta t}{\Delta A_i}\sum_{p=1}^{N_{\mathrm{E}}}\sum_{j=1}^{N_{\mathrm{S}}} f_{p,j}(\mathbf{u}_{\mathrm{R}}, \mathbf{u}_{\mathrm{L}})|\Delta\mathbf{n}_{p,j}| \tag{48}$$

where $f_{p,j}(\mathbf{u}_{\mathrm{R}}, \mathbf{u}_{\mathrm{L}})$ is evaluated at time level n and is defined by Eq. (40) when using any of the schemes defined via Eqs. (41)–(43), respectively, or Eqs. (44) and (47) for the dominant wave scheme. This completes the fundamental approximation of Eq. (37).

9. Higher order schemes without upwinding in two dimensions

Higher order states are based on a MUSCL formalism [20], where the above 1-D principle is extended to two dimensions by constructing higher order data relative to each edge along which flux is to be defined. The higher order left and right hand side states are obtained by expansions about the vertex locations at i and k, Fig. 2. As in 1-D, using maximum principles for a scalar equation, the expansions are constrained with slope limiters in order to prevent the higher order reconstruction from introducing spurious extrema. In this work the reconstruction is performed with respect to the conservative variables. Referring to Fig. 2 the left and right states $\mathbf{u}_{\mathrm{L}}$ and $\mathbf{u}_{\mathrm{R}}$ at the mid-point of the *key* edge e (joining vertices i and k) are expressed as

$$\mathbf{u}_{\mathrm{L}} = \mathbf{u}_i + \frac{1}{2}\Phi^+\Delta\mathbf{u}_{ki} \tag{49}$$

where Φ^+ is a function of

$$\mathbf{r}_{ki}^+ = (\Delta\mathbf{u}_{im}/\Delta\mathbf{u}_{ki}) \tag{50}$$

and

$$\mathbf{u}_{\mathrm{R}} = \mathbf{u}_k - \frac{1}{2}\Phi^-\Delta\mathbf{u}_{ki} \tag{51}$$

where Φ^- is a function of

$$\mathbf{r}_{ki}^- = (\Delta\mathbf{u}_{pk}/\Delta\mathbf{u}_{ki}) \tag{52}$$

where $\Delta\mathbf{u}_{ki} = \mathbf{u}_k - \mathbf{u}_i$ is the edge difference of $\mathbf{u}$. The differences $\Delta\mathbf{u}_{im}$ and $\Delta\mathbf{u}_{pk}$ are only well defined on a structured grid, where the locations of $\mathbf{u}_m$, $\mathbf{u}_p$ would correspond to the next upstream and downstream nodes of the

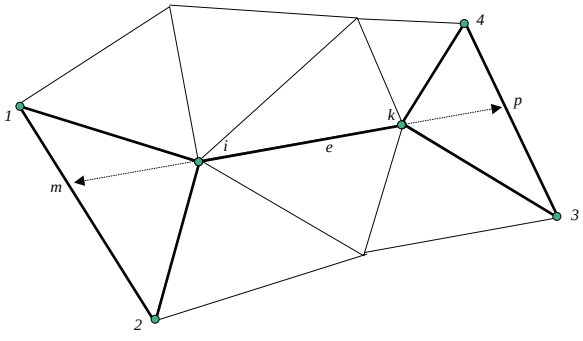

Fig. 2. Higher order edge-based flux support (in bold).

grid, respectively. Extension to unstructured grids requires special construction of the differences $\Delta\mathbf{u}_{im}$ and $\Delta\mathbf{u}_{pk}$.

Two types of definition are considered here for unstructured grids. The first is based directly on [22] with a generalized central gradient defined at the vertex i by $\nabla\mathbf{u}_i$. In this case the gradient of the function is resolved along the direction of the edge and the upstream difference determined from the vertex gradient and edge difference assuming a locally resolved central difference relationship

$$\Delta\mathbf{u}_{im} = 2\nabla\mathbf{u}_i \cdot d\mathbf{r}_{ki} - \Delta\mathbf{u}_{ki} \tag{53}$$

where $d\mathbf{r}_{ki}$ is the edge e space vector with a similar definition for the downstream difference involving the edge difference and gradient at vertex k. While this scheme proves to be quite effective, the scheme lacks formal monotonicity and oscillations can occur in the vicinity of strong shocks, the scheme requires the addition of a maximum–minimum constraints, e.g. as proposed by Barth and Jesperson [23]. Further possibilities are presented in [24].

The second definition which is employed here involves a direct extrapolation of the respective upstream and downstream higher order data which is constrained such that positivity holds for a scalar equation. The upstream triangle $i,1,2$ is labelled T_{U} and the down stream triangle $k,3,4$ is labelled T_{D}. The space vector corresponding to edge e ($d\mathbf{r}_{ki}$) is extrapolated into the respective triangles T_{U}, T_{D}, see arrows in Fig. 2. This is illustrated further with respect to vertex i. The edge vector is extrapolated to the point of intersection m, on the opposite edge of the triangle T_{U}, Fig. 2. The *upwind* difference is then obtained via the expansion

$$\Delta\mathbf{u}_{im} = \nabla\mathbf{u}_{T_{\mathrm{U}}} \cdot d\mathbf{r}_{im} \tag{54}$$

and for a linear approximation of $\mathbf{u}$ over the triangle T_{U} the right hand side of Eq. (54) is equal to the convex average of triangle edge differences with

$$\Delta\mathbf{u}_{im} = (1-\xi)\Delta\mathbf{u}_{i1} + \xi\Delta\mathbf{u}_{i2} \tag{55}$$

where $1-\xi \geqslant 0$ and ξ is the (positive) ratio of area of sub-triangle $i,1,m$ to area of triangle T_{U}. In order to impose a maximum principle with respect to T_{U} and edge e, the limiter Φ^+ is defined so as to bound the higher order gradient approximation by the minimum of the slopes on triangle edges $i1$ and $i2$ and slope of edge e. The limiter is defined by

$$\Phi^+ = \phi(r^+_{ki}) \tag{56}$$

where r^+_{ki} is defined by Eq. (50) and $\phi(r)$ is any standard slope limiter [20] and [21]. The higher order reconstruction is then bounded between $\mathbf{u}_k$ and $\mathbf{u}_m$, by convexity (Eq. (55)) $\mathbf{u}_m = (1-\xi)\mathbf{u}_1 + \xi\mathbf{u}_2$, so that the bounds are between the maximum and minimum of $\mathbf{u}$ over T_{U} and edge e and the reconstruction reduces to first order at two dimensional extrema.

In cases where coincidence or near coincidence is detected between the extrapolated edge and an upwind triangle edge the limiting is collapsed to be entirely edge based. A similar convex average interpolant is constructed for vertex k using the right hand bold triangle together with analogous limiter bounds that now depend on the edge slopes $\Delta\mathbf{u}_{3k}$ and $\Delta\mathbf{u}_{4k}$. After the conservative variable reconstruction an additional test on pressure variation is performed [28], if the local pressure variation is non-physical limiters are set to zero. This completes the definition of the higher order states.

The second step involves selection of the numerical flux according to the chosen scheme and integration via Eq. (48) with the higher order left and right states. In all cases the higher order data is first defined by Eqs. (49), (51) and (54)–(56). The Rusanov based fluxes are defined by (40), together with Eq. (41), (42), or (43). The dominant-wave flux is defined by Eqs. (44), (45) and (47). As in 1-D the Runge–Kutta schemes of [25] can be used to complete the formal time accuracy of the scheme without disturbing spatial operator properties subject to a CFL constraint, here 1/4 is used. These schemes are essentially local edge diminishing LED in motivation [3,24], but applied to the data. As is typical of flux limited schemes, convergence to steady-state is sensitive and limiting is then based on the van-Leer (smooth) limiter, where for positive r

$$\phi(r) = \frac{2r}{(1+r)} \tag{57}$$

and ϕ is zero otherwise. Note as before, that the first order flux is recovered if the limiters are set to zero.

10. Results

10.1. One dimension

The schemes are first compared for the shock tube problem [26] (exact solution solid line, computed square symbol, time = 0.25) with the prescribed initial data

$$(\rho, u, p) = \begin{cases} 1.0, & 0.0, & 1.0 & x \leqslant 0.5 \\ 0.125, & 0.0, & 0.1 & x > 0.5 \end{cases} \tag{58}$$

The higher order scheme results for the Rusanov scheme and dominant wave scheme are shown in Figs. 3 and 4 using 50 nodes. The comparison is only shown for the least diffusive of the non-upwind schemes of Section 8.1, i.e., Rusanov. The LLF scheme result is very close to Rusanov, the GLF result is slightly more diffuse. The comparison for density shows slightly more diffusion at the contact discontinuity computed by the Rusanov scheme,

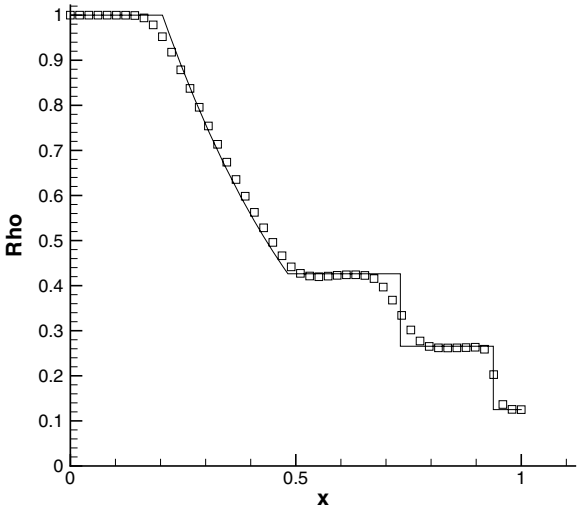

Fig. 3. Shock-tube 50 nodes: higher order Rusanov.

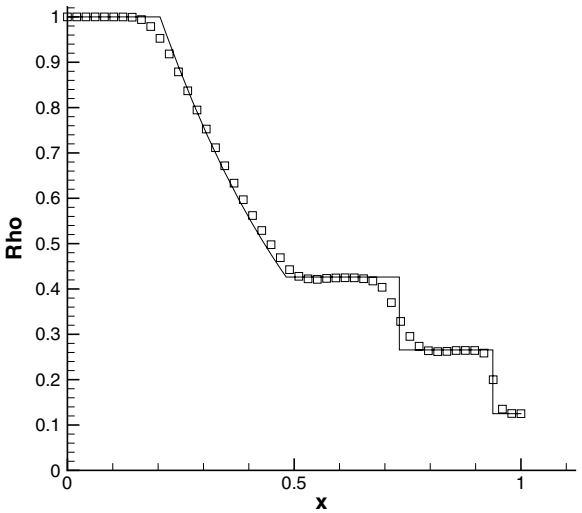

Fig. 4. Shock-tube 50 nodes: higher order dominant-wave.

which is inherent in the method Fig. 3, compared to the dominant wave scheme result (Fig. 4). Both schemes show a significant improvement in resolution using 100 nodes Figs. 5 and 6, consistent with high resolution scheme performance. In this case a 3-shock forms, corresponding to the maximum eigenvalue, so that the Rusanov scheme is well suited to the problem. However, the dominant wave scheme still provides a slightly better overall result due to the improvement in resolution in the region of the contact. The benefit of the dominant wave scheme is particularly striking for the first order scheme comparison Figs. 7 and 8. The lower bound on the dominant wave speed is found to be necessary, primarily in order to resolve the initial jump in data.

10.2. Two dimensions

Results are presented for two types of test case in two dimensions.

The first test is the well known transonic flow over a circular arc, with 10 percent radius, for details, see, e.g. [5]. The initial free stream mach number is specified as 0.675. Subsonic inflow and outflow boundary conditions apply. Data is prescribed according to the number of inward pointing characteristics. Density is updated

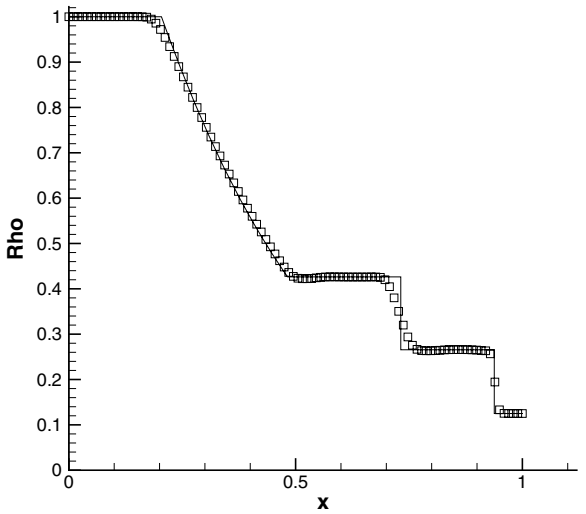

Fig. 5. Shock-tube 100 nodes: higher order Rusanov.

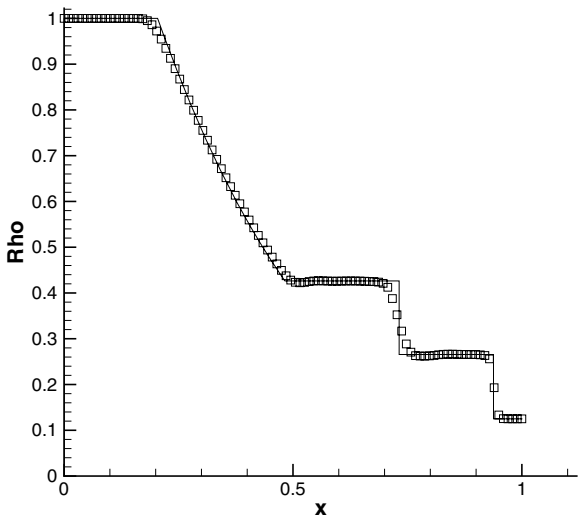

Fig. 6. Shock-tube 100 nodes: higher order dominant-wave.

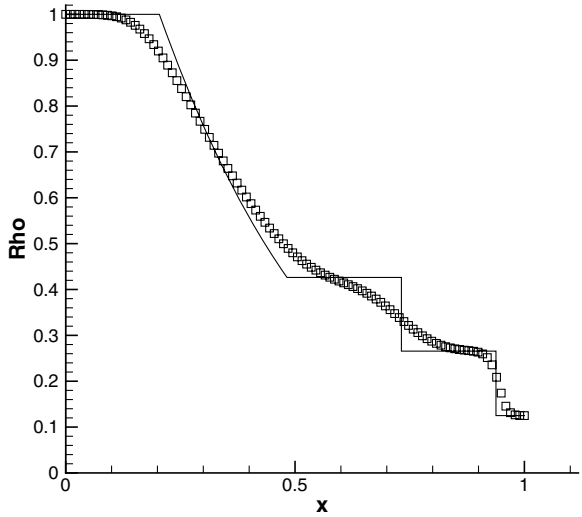

Fig. 7. Shock-tube 100 nodes: first order Rusanov.

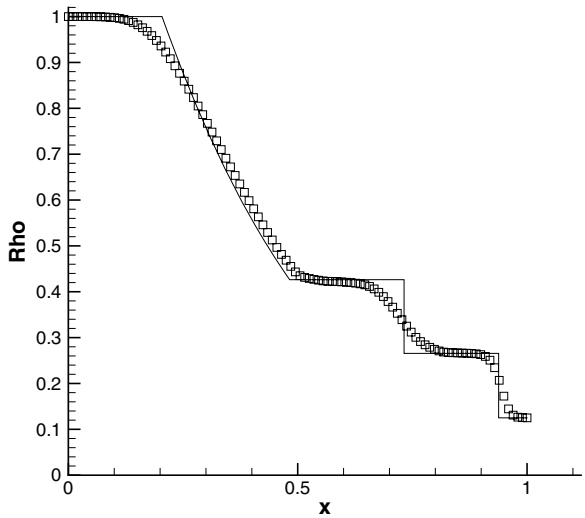

Fig. 8. Shock-tube 100 nodes: first order dominant-wave.

on the inflow boundary (only one outward pointing characteristic) and the pressure is prescribed on the outflow boundary (only one inward pointing characteristic). A weak shock forms on the arc with the shock-foot at 72 percent chord [5]. The triangular grid used for the computational comparisons is shown in Fig. 9. The results are presented in the form of Mach number contours. As in the previous case comparison is only shown between the least diffusive of the non-upwind (Rusanov) schemes and the dominant wave scheme. The higher order Rusanov scheme results are shown in Fig. 10. The diffusive nature of the Rusanov scheme is clearly apparent for this problem, where the weak 1-shock proves to be too weak for the scheme to detect its formation. The additional diffusion based on the largest eigenvalue is clearly inappropriate for such problems, which are actually governed by the smallest eigenvalue of the system. The Rusanov contours only indicate a slight asymmetry in the region of the shock, despite the use of a higher order scheme.

Dominant-wave scheme. In this case the lower bound on the dominant wave speed is found to be essential for computing a stable solution. Moreover, experiments show that the dominant wave speed only requires the lower bound in subsonic flow regions. This is achieved by using

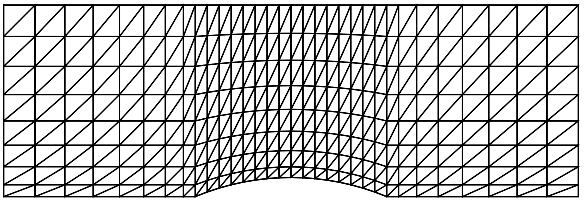

Fig. 9. Channel: grid.

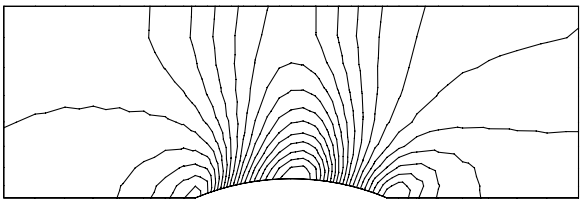

Fig. 10. Mach contours: higher order Rusanov.

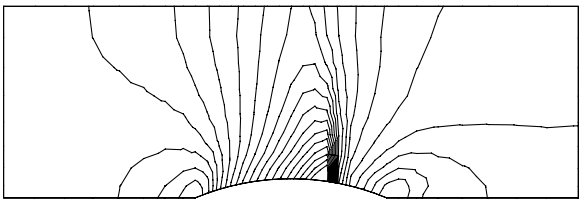

Fig. 11. Mach contours: higher order dominant-wave.

$$|\lambda_{\mathrm{DWB}}| = \begin{cases} \max(|\mathbf{q}\cdot\hat{\mathbf{n}} - a|, |\lambda_{\mathrm{DW}}|) & M < 1 \\ |\lambda_{\mathrm{DW}}| & M \geqslant 1 \end{cases} \tag{59}$$

where M is the local mach number. This condition can be reconciled intuitively since subsonic flow regions are not necessarily dominated by a particular wave. The dominant-wave scheme results of Fig. 11 clearly demonstrate that the new scheme is applicable to transonic flow and can detect the dominant (minimum) eigenvalue in this case, resulting in capture of the shock over the mesh interval that straddles 72 percent chord.

The second case involves supersonic flow over a wedge with 20 degree angle. The initial free stream mach number is specified as 3.0. Supersonic inflow and outflow boundary conditions apply with the vector $\mathbf{u}$ prescribed on inflow boundaries and the solution vector updated on outflow boundaries. Zero normal flow applies on the solid wall. The exact solution is comprised of a strong shock which forms at the corner of the wedge at an angle of 37.5 degrees [27]. Quadrilateral and triangular grids are used for computational comparisons in this study and are shown in Figs. 12 and 13, respectively. The results are presented in the form of density contours.

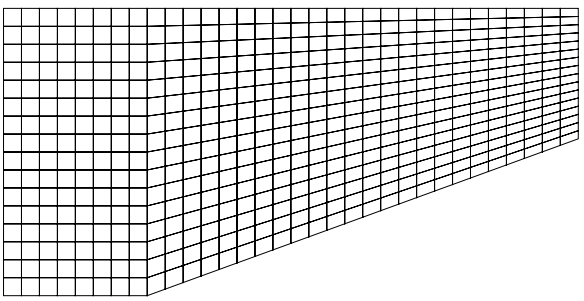

Fig. 12. Wedge: quadrilateral grid.

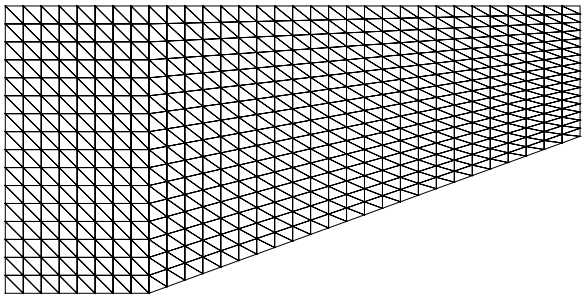

Fig. 13. Wedge: triangular grid.

Quadrilateral results are considered first. The first order scheme comparison Figs. 14 and 15, shows the additional diffusion present in the Rusanov scheme 14. The higher resolution comparison is given in Figs. 16 and 17, the higher order results are quite comparable, with slightly extra diffusion present in the Rusanov result of 16.

The distinction between the schemes is seen to be greater in the case of the triangular grid. The first order scheme comparison Figs. 18 and 19, clearly shows much additional diffusion present in the Rusanov scheme 18, compared to the first order dominant-wave scheme 19. The higher order GLF, LLF and Rusanov scheme results are shown in Figs. 20–22, respectively. The three schemes are each able to resolve the shock in this case, due to the stronger self sharpening nature of the shock. However, the diffusive nature of each scheme is also quite apparent for this problem with some visible spreading of contours. The additional diffusion inherent in these schemes is primarily due to using the modulus of the largest eigenvalue of the system to govern stability of all wave components throughout the field. As expected, the GLF scheme Fig. 22 exhibits the most diffusion due to employing the maximum system eigenvalue over the domain. The LLF scheme result Fig. 23 is close to the Rusanov result Fig. 22, but still slightly more diffusive, due to maximizing over

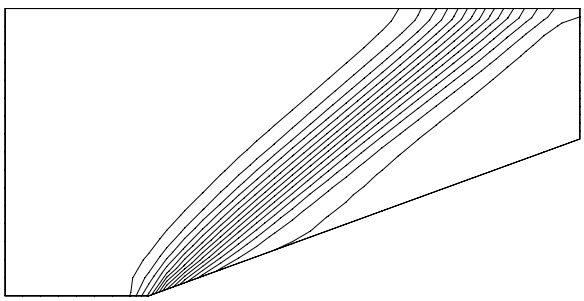

Fig. 14. Density, quad-grid: first order Rusanov.

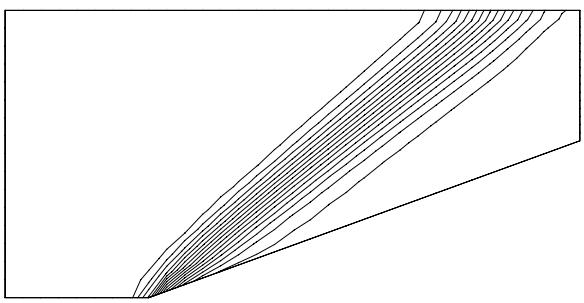

Fig. 15. Density, quad-grid: first order dominant-wave.

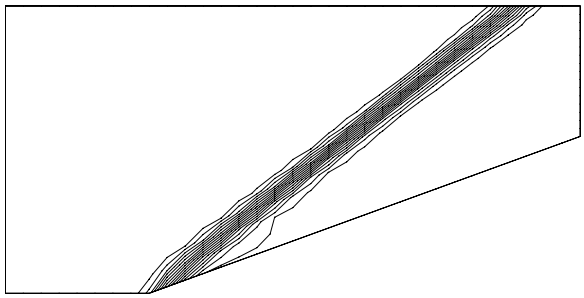

Fig. 16. Density, quad-grid: higher order Rusanov.

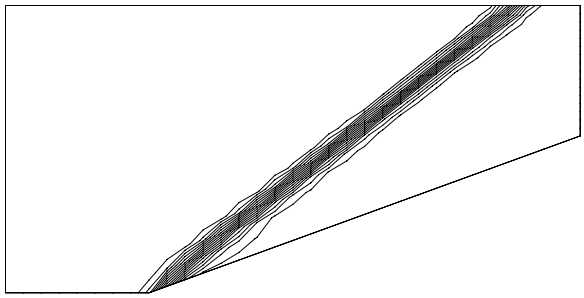

Fig. 17. Density, quad-grid: higher order dominant-wave.

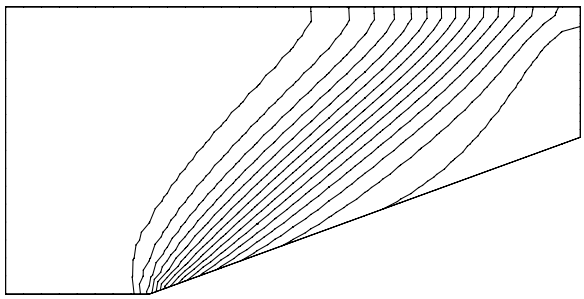

Fig. 18. Density, tri-grid: first order Rusanov.

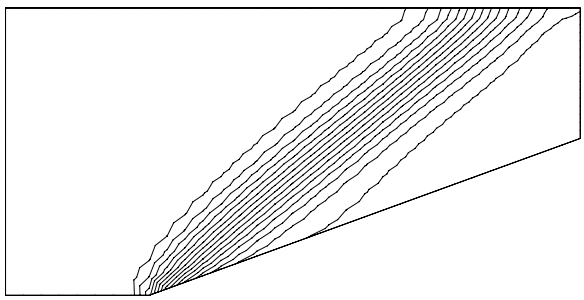

Fig. 19. Density, tri-grid: first order dominant-wave.

the local interval. The higher order dominant-wave scheme result is shown in Fig. 23 and clearly demonstrates an improvement in shock resolution for supersonic flow. This is due to the ability of the new scheme to adjust towards the local dominant wave eigenvalue of the flow, resulting in capture of the shock with less

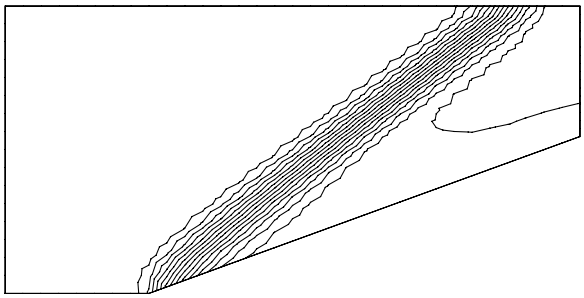

Fig. 20. Density, tri-grid: higher order global Lax–Friedrichs.

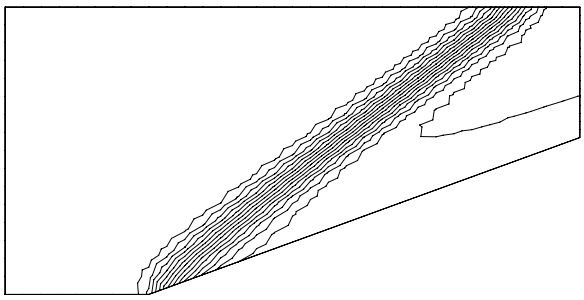

Fig. 21. Density, tri-grid: higher order local Lax–Friedrichs.

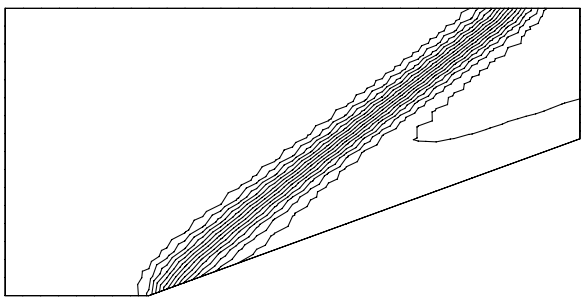

Fig. 22. Density, tri-grid: higher order Rusanov.

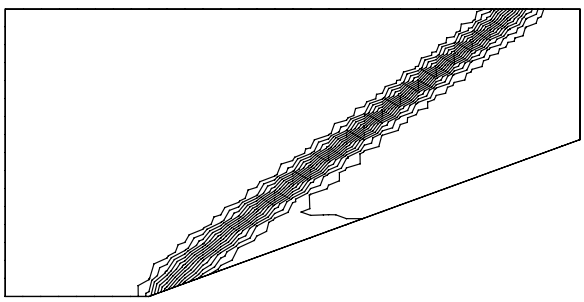

Fig. 23. Density, tri-grid: higher order dominant-wave.

numerical diffusion. The centre line of the band of contours is in line with the exact solution. In this case the dominant-wave scheme works equally well with or without eigenvalue bounds, with no discernable difference found in results.

11. Conclusions

This paper presents a new dominant wave capturing formulation for hyperbolic conservation laws. The method is constructed via a new flux so that local conservation is maintained and is developed within a general finite volume framework. Low order and higher order versions of the method are presented on structured and unstructured grids.

The dominant wave scheme bounded below by the modulus of the smallest eigenvalue of the system performs successfully for all test cases presented and is therefore presented as the current practical version of the method. However tests also show that the bounds are not necessary for all cases.

Comparisons between the new method and the Rusanov, LLF and GLF based schemes reveal clear advantages of the new dominant wave formulation in terms of front resolution.

The schemes are applied to the Euler equations of compressible flow. Results are shown for some classical flow problems. The Rusanov based schemes can either fail to detect discontinuities that are known to be present in the physical solution, or introduce larger amounts of numerical diffusion. In contrast, the new dominant wave scheme is able to capture the discontinuities while using exactly the same grids and equivalent levels of accuracy in terms of polynomial approximation.

The results presented demonstrate the benefits of the dominant wave formulation, and show that improved resolution can be obtained compared to the Rusanov formulation while retaining stability, producing essentially non-oscillatory solutions and continuing to circumvent the need for a characteristic decomposition schemes. The improvement is attributed to the ability of the new scheme to detect the crucial dominant wave eigenvalue of the system and thereby reduce the global numerical diffusion that is added by the Rusanov schemes dependence on the maximum system eigenvalue.

The new flux formulation will be tested with other approximations such as discontinuous Galerkin and ENO in future work. Finally it is noted that the dominant wave formulation offers the potential benefits of being directly applicable to other systems of hyperbolic conservation laws without requiring a characteristic decomposition.

Acknowledgements

I thank the referees for their constructive comments. This work was supported in part by EPSRC Grant GR/S70968/01.

References

[1] E. Godlewski, P. Raviart, Numerical approximation of hyperbolic systems of conservation lawsAppl. Math. Sci., 118, Springer-Verlag, New York, 1996.
[2] P.L. Roe, Approximate Riemann solvers, parameter vectors and difference schemes, J. Comput. Phys. 43 (1981) 357–372.
[3] A. Jameson, Artificial diffusion, upwind biasing, limiters and their effect on accuracy and multigrid convergence in transonic and hypersonic flows, AIAA 93-3359, 1993.
[4] R.W. Maccormack, B.S. Baldwin, A numerical method for solving the Navier–Stokes equations with application to shock-boundary layer interaction, AIAA Paper 75-1, 1975.
[5] R. Ni, A multiple-grid scheme for solving the Euler equations, AIAA J. 20 (11) (1982) 1565–1571.
[6] A. Jameson, W. Schmidt, E. Turkel, Numerical simulation of the Euler equations by finite volume methods using Runge–Kutta time stepping schemes, AIAA Paper 81-1259, 1981.
[7] R.C. Swanson, E. Turkel, On central-difference and upwind schemes, J. Comput. Phys. 101 (1992) 297–306.
[8] T.H. Pulliam, J. Steger, Recent improvements in efficiency accuracy and convergence for implicit approximate factorization algorithms, AIAA No. 85-0360, 1985.
[9] R. Lohner, K. Morgan, O. Zienkiewicz, The solution of non-linear hyperbolic equation systems by the finite element method, IJNMF 4 (1984) 1043–1063.
[10] S.F. Davis, TVD finite difference schemes and artificial viscosity, ICASE Report No. 84-20, 1984.
[11] H.C. Yee, Construction of explicit and implicit symmetric TVD schemes and their applications, J. Comput. Phys. 68 (1987) 151–179.
[12] H. Nessyahu, E. Tadmor, Non-oscillatory central differencing for hyperbolic conservation laws, J. Comput. Phys. 87 (1990) 408–463.
[13] X.D. Liu, S. Osher, Convex ENO high order multi-dimensional schemes without field by field decomposition or staggered grids, J. Comput. Phys. 141 (1998) 1–27.

[14] X.D. Liu, P. Lax, Positive Schemes for solving multi-dimensional hyperbolic systems of conservation laws, J. Comput. Phys. 187 (2003) 428–440.
[15] H. Yu, Y.P. Liu, A second order accurate, component-wise TVD scheme for non-linear, hyperbolic conservation laws, J. Comput. Phys. 173 (2001) 1–16.
[16] M.G. Edwards, Moving element methods with emphasis on the Euler equations, Ph.D. Thesis, Mathematics Department, Reading University, UK, 1987.
[17] M.G. Edwards, The dominant wave-capturing finite-volume scheme for systems of hyperbolic conservation laws, in: Proceedings of the European Congress on Computational Methods in Applied Sciences and Engineering, Jyvaskyla, 24–28 July, 2004.
[18] V.V. Rusanov, Calculation of interaction of non-steady shock waves with obstacles, Zhur Vychislitel noi Mathematicheskoi Fiziki 1 (1961) 267–279.
[19] A. Harten, J.M. Hyman, Self adjusting grid methods for one dimensional hyperbolic conservation laws, J. Comput. Phys. 50 (1983) 235–269.
[20] B. van Leer, Towards the ultimate conservative difference scheme V. A sequel to Godunov's method, J. Comput. Phys. 32 (1979) 101–136.
[21] P. Sweby, High resolution schemes using flux limiters for hyperbolic conservation laws, SIAM J. Numer. Anal. 21 (1984) 995–1011.
[22] L. Fezou, B. Stoufflet, A class of implicit upwind schemes for Euler simulations with unstructured meshes, J. Comput. Phys. 84 (1989) 174–206.
[23] T.J. Barth, D. Jesperson, The design and application of upwind schemes on unstructured meshes, AIAA Paper 89-0366, 1989.
[24] P. Lyra, K. Morgan, A review and comparative study of upwind biased schemes for compressible flow computation. Part III: Multidimensional extension on unstructured grids, Arch. Comput. Meth. Eng. 9 (3) (2002) 207–256.
[25] C.W. Shu, S. Osher, Efficient implementation of essentially non-oscillatory shock capturing schemes, J. Comput. Phys. 77 (1988) 439–471.
[26] G.A. Sod, A survey of several finite difference methods for systems of non-linear hyperbolic conservation laws, J. Comput. Phys. 27 (1978) 1–31.
[27] R. Courant, K.O. Friedrichs, Supersonic flow and shock waves, Appl. Math. Sci., 21, Springer-Verlag, New York, 1948.
[28] P. Batten, C. Lambert, D.M. Causon, Positively conservative high-resolution convection schemes for unstructured elements, Int. J. Numer. Meth. Eng. 39 (11) (1996) 1821–1838.